PCCP

PAPER

View Article Online
View Journal | View Issue

Cite this: *Phys. Chem. Chem. Phys.*, 2018, **20**, 24239

n- and p-type ohmic contacts at monolayer gallium nitride–metal interfaces†

Ying Guo, *[ab] Feng Pan,[a] Yajie Ren,[a] Binbin Yao,[a] Chuanghua Yang,[a] Meng Ye,[c] Yangyang Wang,[d] Jingzhen Li,[b] Xiuying Zhang,[b] Jiahuan Yan,[b] Jinbo Yang[be] and Jing Lu*[be]

Received 26th July 2018,
Accepted 28th August 2018

DOI: 10.1039/c8cp04759f

rsc.li/pccp

Recently, two-dimensional (2D) gallium nitride (GaN) was experimentally fabricated, and has promising applications in next-generation electronic and optoelectronic devices. A direct contact with metals to inject the carrier is often required for potential 2D GaN devices. Herein, the first systematic study on the interface properties of monolayer (ML) planar and buckled GaN with different metal electrodes (Al, Ti, Ag, Au, Sc, and Pt) in a field-effect transistor framework is presented using first-principles energy band calculations and quantum transport simulations. Because of moderate Fermi level pinning (electron pinning factor S_L^e = 0.63), ML planar GaN and the Ag electrode form an n-type lateral Schottky contact, while ML planar GaN and Ti, Al, and Au electrodes form a p-type lateral Schottky contact. The ML buckled GaN, Ag, Al, Ti, and Sc electrodes form a p-type lateral Schottky contact as a result of Fermi level pinning with a hole pinning factor of S_L^h = 0.75. Notably, a highly desirable n-type/p-type lateral ohmic contact is formed at the lateral interface of the ML planar GaN and Sc/Pt electrodes, and a p-type lateral ohmic contact is formed at the lateral interface of the ML buckled GaN and Pt/Au electrodes. Therefore, a low resistance contact can be realized in ML planar and buckled GaN devices.

1. Introduction

Semiconducting group III nitride materials, such as gallium nitride (GaN), have been intensively studied for many years[1–6] since they have extensive applications in high efficiency electronic and optoelectronic equipment such as high electron mobility transistors, light-emitting diodes, and laser diodes.[7–10] In addition, two-dimensional (2D) semiconductors such as 2D transition-metal dichalcogenides (TMDC) with band gaps in the range of 1–2 eV and 2D group-V-enes (phosphorene, arsenene, antimonene, and bismuthene) with band gaps in the range of 0–2.62 eV[11–17] are attracting increasing attention. Compared with 3D semiconductors, 2D materials easily stack in the vertical direction and are controlled by a gate; also, there are few traps on the interface of semiconductor-dielectrics. Therefore, 2D materials are potential channel materials for next-generation electronic and optoelectronic devices.[18–21] Currently, sub-10 nm 2D MoS_2 field-effect transistors (FETs) have been synthesized by several groups, with gate lengths scaled down to 1 nm[14] or channel lengths scaled down to 4 nm.[22–24]

Recently, 2D GaN was manufactured by a migration-enhanced encapsulated growth technique.[25] The 2D semiconductor material GaN has two types of hexagonal structures after relaxation according to theoretical studies: a planar structure and a buckled structure.[1,25] The 2D planar structure has unsaturated states with an indirect band gap of 2.17 eV.[26–28] The buckled structure is properly passivated using partially charged pseudo-hydrogen, and has a direct band gap of 5.28 eV.[25] ML GaN appears quite promising as a 2D semiconductor in electronics and optoelectronics applications considering the extensive applications of its 3D counterpart. In an actual 2D material device, the metal electrode directly contacts the 2D material causing an influx of carriers owing to the lack of a proper doping approach; moreover, a Schottky barrier usually appears at the interface of 2D semiconductor–metal contacts as a result of the Fermi level pinning effect.[11–13] The Schottky barrier always lowers the device performance significantly because of the production of an extra contact resistance, which slows the carrier speed.

In this study, we used first-principles energy band and quantum transport simulation to perform the first comprehensive study on the interfacial properties between electrodes

[a] *School of Physics and Telecommunication Engineering, Shaanxi Key Laboratory of Catalysis, Shaanxi University of Technology, Hanzhong 723001, P. R. China. E-mail: guosophia@163.com*
[b] *State Key Laboratory of Mesoscopic Physics and Department of Physics, Peking University, Beijing 100871, P. R. China. E-mail: jinglu@pku.edu.cn*
[c] *State Key Laboratory for Superlattices and Microstructures, Institute of Semiconductors, Chinese Academy of Sciences, 100083, P. R. China*
[d] *Nanophotonics and Optoelectronics Research Center, Qian Xuesen Laboratory of Space Technology, China Academy of Space Technology, Beijing 100094, P. R. China*
[e] *Collaborative Innovation Center of Quantum Matter, Beijing 100871, P. R. China*
† Electronic supplementary information (ESI) available. See DOI: 10.1039/c8cp04759f

(Al, Ti, Ag, Au, Sc, and Pt) and the hexagonal ML GaN planar structure (labeled as ML planar GaN) and buckled structure (labeled as ML buckled GaN) in the FET configuration. After contact with metals, ML planar GaN undergoes metallization in the vertical direction. However, owing to moderate Fermi level pinning (electron pinning factor S_L^e = 0.63), the metalized ML planar GaN and channel ML planar GaN form a lateral Schottky barrier. Moreover, the band structure of ML buckled GaN is clearly identifiable after contact with metal electrodes. Owing to Fermi level pinning with a hole pinning factor of S_L^h = 0.75, ML buckled GaN and Ag, Al, Ti, and Sc electrodes form a p-type vertical and lateral Schottky contact. Remarkably, ML planar GaN and Sc and Pt electrodes form a highly desirable n-type and p-type lateral ohmic contact, and ML buckled GaN and Pt and Au electrodes form a p-type vertical and lateral ohmic contact.

2. Computational details

Fig. 1(a) shows the top-view (top panel) and side-view (bottom panel) of hexagonal ML planar GaN, and the optimized lattice parameter of ML planar GaN is a = 3.24 Å, which is in agreement with the previously calculated values.[2,27,28] Fig. 1(b) shows the top-view (top panel) and side-view (bottom panel) of the ML buckled GaN buckling honeycomb lattice. The lattice parameter of hexagonal ML buckled GaN is a = 3.18 Å, and the buckling height is denoted as Δ (0.75 Å), as shown in the side-view. Six commonly used metals (Sc(0001), Ti(0001), Ag(111), Al(111), Au(111), and Pt(111)) were considered as electrodes, and their work function varies from 3.06 to 5.50 eV. We adapted the lattice constant of the metal electrode to that of ML GaN. The mismatch of the lattice constant varies from 0.75% to 5.18%, as shown in Table 1. Six atomic layers were chosen to simulate the metal electrodes, and the atomic positions of the bottom layer of the metal electrode was fixed and the top five layers were relaxed because the interaction chiefly occurs between ML GaN and the metal atoms of the top layer. To avoid false interaction in the periodic structures, we chose more than 15 Å along the z-axis as a vacuum buffer space.

We used the plane-wave pseudopotential density functional theory (DFT) calculation implemented in the Vienna ab initio simulation package (VASP)[29,30] for geometry optimization (relaxation) and calculation of the electronic structures. The projector-augmented-wave (PAW) potential was used to describe the electron–ion interaction. For geometry optimization, 9 × 9 × 1 k-point Monkhorst meshes were sampled in the Brillouin integration, and an energy cutoff of 400 eV was used. In the energy band calculation, 24 × 24 × 1 k-point Monkhorst meshes were sampled in the Brillouin integration, and an energy cutoff of 500 eV was used. The atomic locations were fully relaxed until the maximum force was below 0.001 eV Å^{-1} per atom and the convergence standard for energy was within 1 × 10^{-6} eV per atom. The DFT-D2 method of Grimme[31,32] was used to simulate the van der Waals interactions between ML GaN and the metal electrodes. In the z-direction, a dipole correction was adopted to avoid the pseudo effect[33] by asymmetry in the combined systems. The ultrasoft pseudopotential plane-wave method[34,35] implemented in the CASTEP code[36] was used to calculate the total electron density and the charge transfer (Mulliken population analysis), and a plane-wave energy cutoff of 400 eV was used.

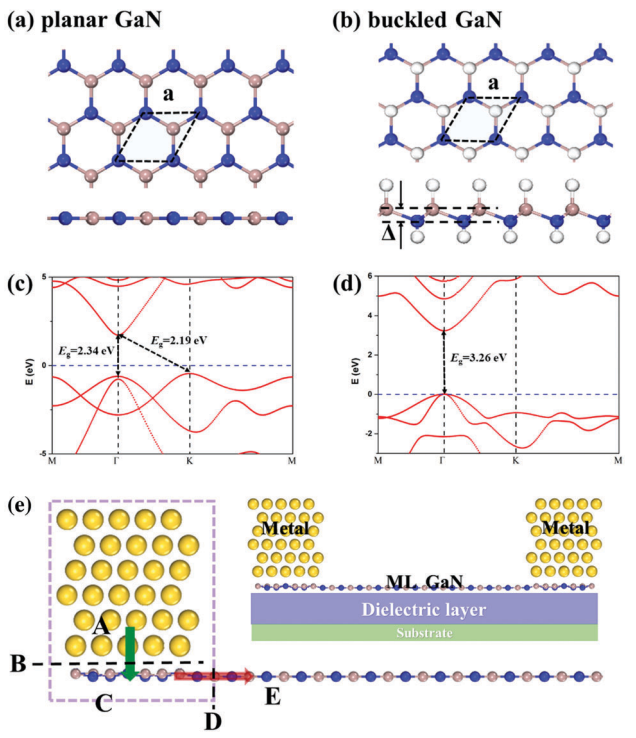

Fig. 1 (a and b) Top- and side-view of the free-standing ML planar/buckled GaN, respectively. The rhomboid represents the unit cell. (c and d) Band structure of ML planar/buckled GaN, respectively. (e) Schematic cross-sectional view of a typical intrinsic ML GaN in contact with a metal. B is the vertical interface between the metal and underlying ML GaN, and D is the lateral interface between the contacted and uncontacted ML GaN. The arrows denote the pathway (A → B → C → D → E) of electron or hole injection from the contact metal (A) to the channel ML GaN (E). Inset: An ML GaN FET.

Table 1 Calculated geometry structures of the ML GaN–metal contacts. $\bar{\varepsilon}$ is the lattice mismatch between the metals and ML GaN, d_0 the vertical distance from the bottom GaN atom layer to the topmost metal atom layer, and d_{min} the minimum distance of atom to atom from GaN to the metals. Δ is the vertical distance from the topmost layer to the bottom atom layer of ML GaN in contact with metal electrodes, and Δ_M the height of buckling for the topmost metal layer of the combined systems. E_b is the binding energy (each GaN atom) needed to remove the ML GaN layer from the metal electrodes

Metal		Al	Ag	Au	Sc	Ti	Pt
Planar GaN	$\bar{\varepsilon}$ (%)	1.37	1.97	1.85	1.42	3.44	0.75
	d_0 (Å)	1.97	2.65	2.59	2.17	0.67	2.13
	d_{min} (Å)	1.97	2.68	2.59	2.29	1.92	2.13
	Δ (Å)	0.73	0.17	0.42	0.13	2.00	0.87
	Δ_M (Å)	0.090	0.571	0.086	0	0.70	0.099
	E_b (eV/GaN)	0.49	0.56	0.59	1.28	2.67	1.07
Buckled GaN	$\bar{\varepsilon}$ (%)	2.55	3.12	3.00	3.00	5.18	0.49
	d_0 (Å)	2.60	2.24	2.33	2.35	2.17	2.20
	d_{min} (Å)	2.76	2.43	2.50	2.98	2.84	2.39
	Δ (Å)	0.834	0.721	0.746	0.740	0.739	0.743
	Δ_M (Å)	0	0	0	0	0	0
	E_b (eV/GaN)	0.18	0.31	0.34	0.27	0.33	0.42

Fig. 1(e) shows a schematic cross-sectional view of the interface model for the ML GaN device, and the electrode region comes from the optimized ML GaN/metal combined systems. This type of interface model has been used for 2D material (TMDC, 2D group-V-enes, and 2D group-IV-enes)/metal-combined systems.[11,15,37–40] There exist two interfaces in the device interface model. One is the vertical interface (interface B) between ML GaN and the metal electrode and the other is the lateral interface (interface D) between the channel and region of ML GaN.

The ML GaN FET uses a two-probe model by the channel (about 5 nm pure ML GaN) and two electrode (ML GaN/metal semi-infinite combined systems) regions. The local density of states and transport properties of FET were calculated *via* the DFT method and non-equilibrium Green's function (NEGF) coupled in the ATK 2017 package. In the channel and electrodes region of the FET, $50 \times 1 \times 1$ ($k_x \times k_y \times k_t$) and $50 \times 1 \times 50$ k-point Monkhorst meshes were sampled in the irreducible Brillouin zone (IBZ). k_t is the number of k-points along the transport direction; $k_t = 1$ in the channel region (aperiodic direction) and $k_t = 50$ in the electrode region (period infinite direction). A large number of k-points ($k_t = 50$) along the transport direction for the electrode calculation is crucial to achieve convergence and accuracy during the device simulation because it ensures that the electronic structures (particularly the Fermi level) match properly at the electrode-channel region boundaries.[41] To ensure electron/hole neutrality in the electrode region, the Dirichlet boundary condition was used at the lateral interface, and the Neumann boundary condition was used at the vertical interface. The temperature was 300 K and the double-ζ polarized (DZP) basis set was used with the FHI pseudopotentials.

The transmission coefficient T (k_x, E; k_x is a vector orthogonal to the transport direction) in the IBZ of the reciprocal lattice is derived from the following expression:

$$T(k_x,E) = T_r(G^r(k_x,E)\Gamma_L(k_x,E)G^a(k_x,E)\Gamma_R(k_x,E)) \quad (1)$$

where $G^r(k_x,E)$ ($G^a(k_x,E)$)is the retarded (advanced) Green function and $\Gamma_{L(R)}(k_x,E) = i(\Sigma^r_{L(R)}(k_x,E) - \Sigma^a_{L(R)}(k_x,E))$ reflects the level broadening by the left electrode/right electrodes expressed according to the electrode self-energies $\Sigma^r_{L(R)}(E)$, which reflect the effect of the electrodes on the scattering region. At a given energy, $T(E)$ is the average of $T(k_x,E)$ over 50 k_x-points.

The exchange–correlation functional employed the generalized gradient approximation (GGA) proposed by Perdew–Burke–Ernzerhof (PBE). This type of single-electron approximation is effective enough to simulate the electron behavior in calculations for FET devices because the electron–electron interaction of the 2D semiconductor channel is restrained by carriers from the metal electrodes. This effectiveness is confirmed from the agreement between the calculated and experimental transport gaps (0.68, 0.81, and 0.65 *versus* 0.61, 0.71, and 1.0 eV) for trilayer, bilayer and ML black phosphorene FET, respectively.[13,42–45] Furthermore, when an Ni electrode is used in phosphorene FETs, the hole (electron) SBH at the DFT-GGA level[43] is also consistent with the experimental value.[46]

3. Results and discussion

3.1 Electronic structures of the ML GaN and metal interfacial systems

There were three initial structures of ML GaN/metal adopted at the beginning of relaxation: N(N–H) atoms on the top, hollow fcc, and hollow hcp surface sites. The most appropriate configurations of the ML GaN/metal contact interfaces are shown in Fig. 2. The honeycomb structure of ML GaN is well-preserved except for ML planar GaN in contact with Ti, as shown in Fig. 2(e). In addition, some atoms of ML planar GaN slightly depart from their original locations in the vertical direction, with Δ of 0.13, 0.17, 0.42, 0.66, and 0.87 Å in ML planar GaN/Sc/Ag/Au/Al/Pt, respectively. In contrast, the ML GaN contacted with Ti is remarkably deformed with Δ = 2.00 Å. The heights of

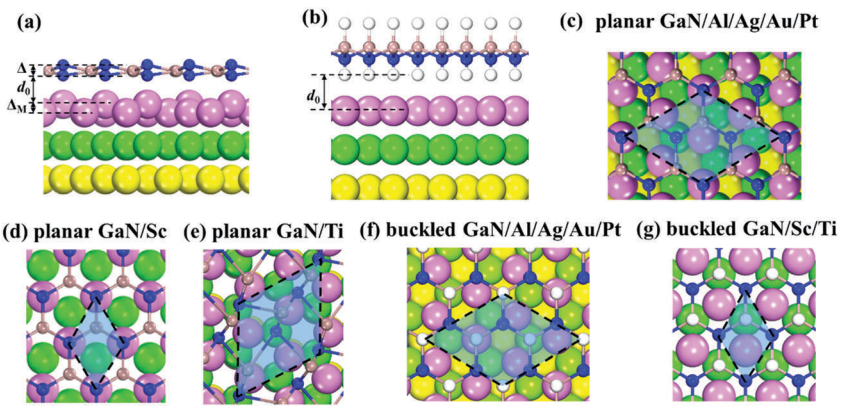

Fig. 2 (a and b) Schematic side-views of ML planar/buckled GaN on metals. (c) Top-views of the stable configuration for ($\sqrt{3} \times \sqrt{3}$) ML planar GaN on (2 × 2) Al(111)/Ag(111)/Au(111) and Pt(111). (d and e) Top-view of the stable configuration for ML (1 × 1) planar GaN on the (1 × 1) Sc(001) and Ti(001) electrodes, respectively. (f) Top-views of the stable configuration for ($\sqrt{3} \times \sqrt{3}$) ML buckled GaN on (2 × 2) Al(111)/Ag(111)/Au(111) and Pt(111). (g) Top-view of the stable configuration for ML (1 × 1) buckled GaN on (1 × 1) Sc(001)/Ti(001). The N, Ga and H atoms are in blue, light brown, and white, respectively. Light purple, green and yellow indicate the first layer atoms, second layer atoms and third layer atoms of the metals, respectively. The black diamonds represent the unit cells.

ML buckled GaN contacted with Au/Ti/Sc/Pt are almost in agreement with that of free-standing ML buckled GaN (Δ = 0.75 Å), while the height of ML buckled GaN contacted with Al and Ag is 0.83 and 0.72 Å, respectively. The topmost atom layer of the metal electrodes with ML buckled GaN and Sc with ML planar GaN is flat, but the topmost atom layer of Au, Al, Pt, Ag, and Ti with ML planar GaN are buckled, with heights of 0.086, 0.09, 0.099, 0.571, and 0.70 Å, respectively (Table 1).

The initial interfacial distance from the bottommost ML GaN to the topmost metal electrode layer is d_0 = 3 Å. Finally, the d_0 of ML planar GaN contacted with Al, Pt, Sc, Au, and Ag are 1.97, 2.13, 2.17, 2.59, and 2.56 Å, respectively, while ML planar GaN contacted with Ti has an extraordinarily small d_0 of 0.67 Å. The d_0 value is within the range of 2.17–2.60 Å for ML buckled GaN contacted with metals (as shown in Table 1). d_{min} is the minimum atom-to-atom interval between the metal and ML GaN. d_{min} of ML planar GaN contacted with Al/Au/Pt has a similar value to d_0, while d_{min} of ML planar GaN contacted with Ti, Sc, and Ag is 1.92, 2.29 and 2.68 Å, respectively, which is larger than their respective d_0. The d_{min} value of ML buckled GaN contacted with Pt, Ag, Au, Al, Ti, and Sc is 2.39, 2.43, 2.50, 2.76, 2.84, and 2.98 Å, respectively, which are all larger than their respective d_0 values (Fig. 3).

We optimized the ML planar GaN/Ag interface using both ATK and VASP codes (as shown in Fig. S1, ESI†), and the Δ, Δ_m, and d_0 of the interfacial system calculated by ATK (VASP) are 0.14 (0.17), 0.075 (0.089) and 2.53 (2.65) Å, respectively. Therefore, the equilibrium structures of the ML planar GaN–Ag interface optimized by the two codes are quite similar.

The binding energy per interfacial ML GaN atom is defined as

$$E_b = (E_{GaN} + E_{metal} - E_{GaN/metal})/N_{GaN} \quad (2)$$

where E_{GaN}, E_{metal}, and $E_{GaN/metal}$ are the energies of ML GaN, pure metal electrode, and the combined system per supercell, respectively, after relaxation. N_{GaN} is the number of GaN atoms per supercell.

The E_b values (eV) for the different ML planar GaN combined systems increase in the order Al (0.49) < Ag (0.56) < Au (0.59) < Pt (1.07) < Sc (1.28) < Ti (2.67). The particularly large binding energy between ML GaN and Ti is attributed to the large deformation of ML GaN on Ti. According to the binding energy data, strong chemical bonding occurs between ML planar GaN and Sc/Pt with smaller interfacial distance, d_0, (2.13/2.17 Å) and minimum atom-to-atom distance, d_{min} (2.13/2.29 Å). However, ML planar GaN and Al/Ag/Au form weak chemical bonds with larger d_0 (2.65 (Ag) and 2.59 (Au) Å) and d_{min} (2.68 (Ag) and 2.59 (Au) Å), except for Al (d_0 = 1.97 Å and d_{min} = 1.97 Å) (Table 1).

The different electronic structures of the different metals lead to different binding strengths in the ML planar GaN/metal combined systems. The E_b values of the Al (atom ($3s^2p^1$)), Ag (atom ($4d^{10}5s^1$)) and Au (atom ($5d^{10}6s^1$)) electrodes and ML planar GaN combined systems are low because these elements have only one unpaired electron and form one covalent bond with ML planar GaN. However, the Pt atom ($5d^96s^1$), Sc atom ($3d^14s^2$), and Ti atom ($3d^24s^2$) have two, three, and four unpaired electrons, and they form two, three, and four covalent bonds with ML planar GaN, respectively. Therefore, the E_b values of these three combined systems are large, and increase in the order Pt < Sc < Ti.

A weak interaction is always formed between ML buckled GaN and metal electrodes with an increase in d_{min} (2.43–2.98 Å) and d_0 (2.17–2.60 Å) (Table 1). The E_b values (eV) increase in the order Al (0.18) < Sc (0.27) < Ag (0.31) < Ti (0.33) < Au (0.34) < Pt (0.42). For the same metal electrode, the binding strength of ML buckled GaN is always weaker than that of ML planar GaN because the dangling bond is saturated in ML buckled GaN and no covalent bond is available.

Fig. 4 shows the total electron distributions of ML GaN/metal in real space. It is clearly shown that electrons are accumulated in the interface, indicating that the ML planar GaN and metal electrodes form a covalent bond. The levels of electron accumulation at the interfaces of ML planar GaN and Ag, Al, and Au electrodes are lower than that at the interfaces of ML planar GaN and Sc, Ti, and Pt electrodes, which is in agreement with the levels of the binding intensity. The amount of shared density at the interface of ML buckled GaN and metals is much smaller than that at the interface of ML planar GaN and metals, which indicates van der Waals interactions in the ML buckled GaN/metal combined systems. The Mulliken population analysis reveals that every pair of GaN atoms in ML

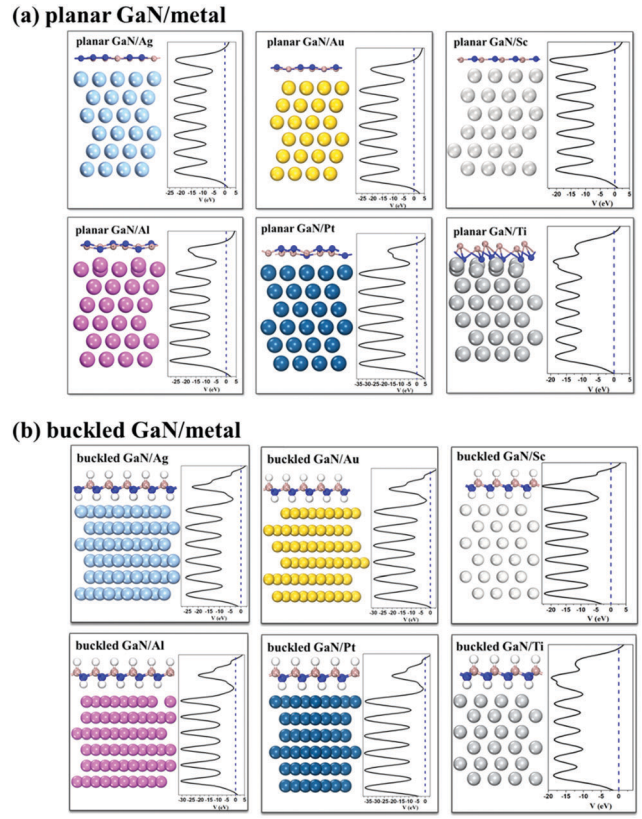

Fig. 3 (a and b) Side-views of the geometrical structures and average electrostatic potentials (AEP) of ML planar/buckled GaN on the Ag, Au, Sc, Al, Pd, and Ti electrodes, respectively. The Fermi level is at zero energy.

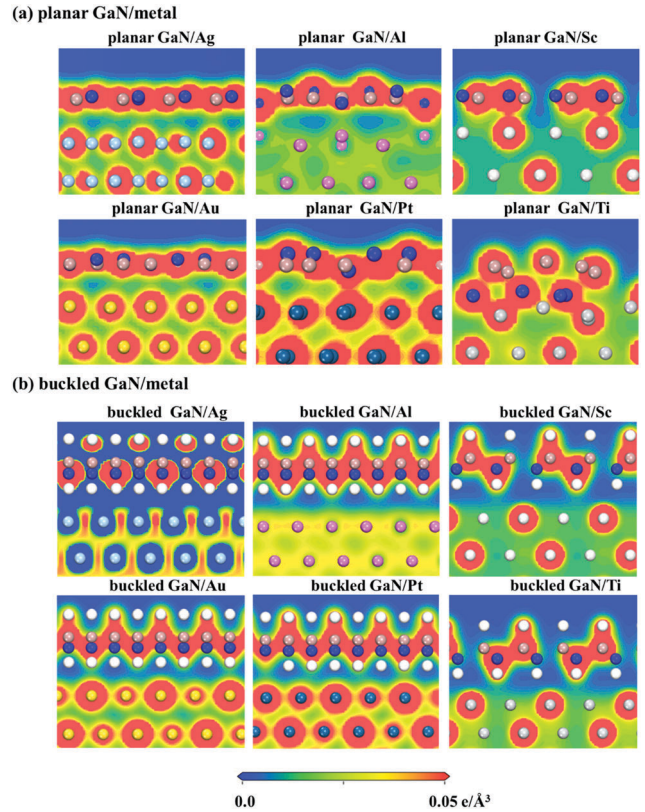

Fig. 4 (a and b) Electron density difference of ML planar/buckled GaN on the Ag, Al, Sc, Au, Pt, and Ti electrodes, respectively. The color scale is shown below the plot.

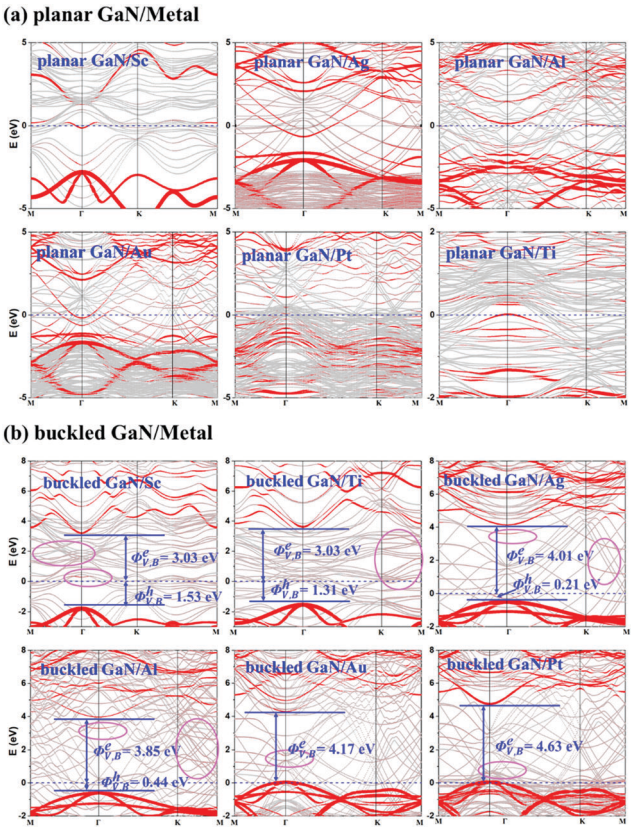

Fig. 5 (a and b) Energy band structures of ML planar/buckled GaN on the Sc, Ag, Al, Au, Pt, and Ti electrodes. Gray dots correspond to the GaN/metal system. Red dots correspond to the states with valid contribution from ML GaN, and the radii of the dots are proportional to the weight. Light purple closed area indicates the region with MIGS. The Fermi level is at zero energy.

planar GaN gets 0.02, 0.047, 0.05, 0.27, and 0.537 electrons on the Pt, Al, Ag, Sc, and Ti electrodes, respectively, and loses 0.017 electrons on the Au electrode (Table 1). Hence, the bond type between ML planar GaN and Sc and Ti electrodes is a mixed covalent bond and charge transfer interaction. Moreover, every pair of GaN atoms in ML buckled GaN gets 0.00, 0.02, 0.03, 0.04, and 0.07 electrons on Au, Pt, Ag, Sc, and Ti electrodes, respectively, and loses 0.027 electrons on the Al electrode.

In the band structures of the ML GaN/metal combined systems (Fig. 5), the band of GaN is denoted by the red dots, in which radii represents the weight of the GaN atoms in the combined systems. In the ML planar GaN/metal combined systems, a covalent bond is formed because the bands of ML planar GaN supported by metal electrodes are strongly hybridized. The Fermi level always intersects the bands of ML planar GaN and thus, ML planar GaN on the six electrodes undergoes metallization. However, the band gap (E_g) of ML buckled GaN is clearly identifiable after contact with the metal electrodes, which is typical of weak van der Waals interaction. Fig. 5(b) shows that ML buckled GaN and Ag, Al, Ti, and Sc electrodes form a p-type vertical Schottky contact, which has a hole SBH of 0.21, 0.44, 1.31, and 1.53 eV, respectively. Remarkably, the Au and Pt electrodes form a p-type vertical ohmic contact. The band gaps in the vertical direction are 4.17 (Au), 4.22 (Ag), 4.29 (Al), 4.34 (Ti), 4.56 (Sc), and 4.63 (Pt) eV, which are all larger than the gap (3.26 eV) of free-standing ML buckled GaN at the GGA level (VASP). We identified the GaN-derived states within the band gap of ML buckled GaN as metal-induced gap states (MIGS).

To explore the cause of these changed band gaps in the ML buckled GaN/metal combined systems, we calculated the band structures of only ML buckled GaN peeled from the Al, Ag, Au, Pt, Sc, and Ti electrodes, as shown in Fig. S2 (ESI†). The structures and the band gaps of ML buckled GaN are almost the same as that of the free-standing ML buckled GaN, and the direct band gaps are almost 3.12 eV, which are comparable with that of the free-standing ML buckled GaN ($E_{g\text{-direct}}$ = 3.26 eV). Therefore, it is the interaction with the metal electrodes that enlarges the energy band of ML buckled GaN. This interaction is tentatively attributed to the repulsion between the intensive metal states in the middle of the band gap and the conduction and valence band of ML buckled GaN.

The cumulative partial density of states (PDOS) on the GaN atoms of ML GaN/metals are shown in Fig. 6, which further verify the metallization of ML planar GaN and the semiconducting nature of ML buckled GaN on the six metal electrodes. After contact with the metal electrodes, the band gap of ML planar GaN disappears (Fig. 6(a)) and an ohmic infusion of carriers is revealed in the vertical direction for all the ML planar GaN/metal

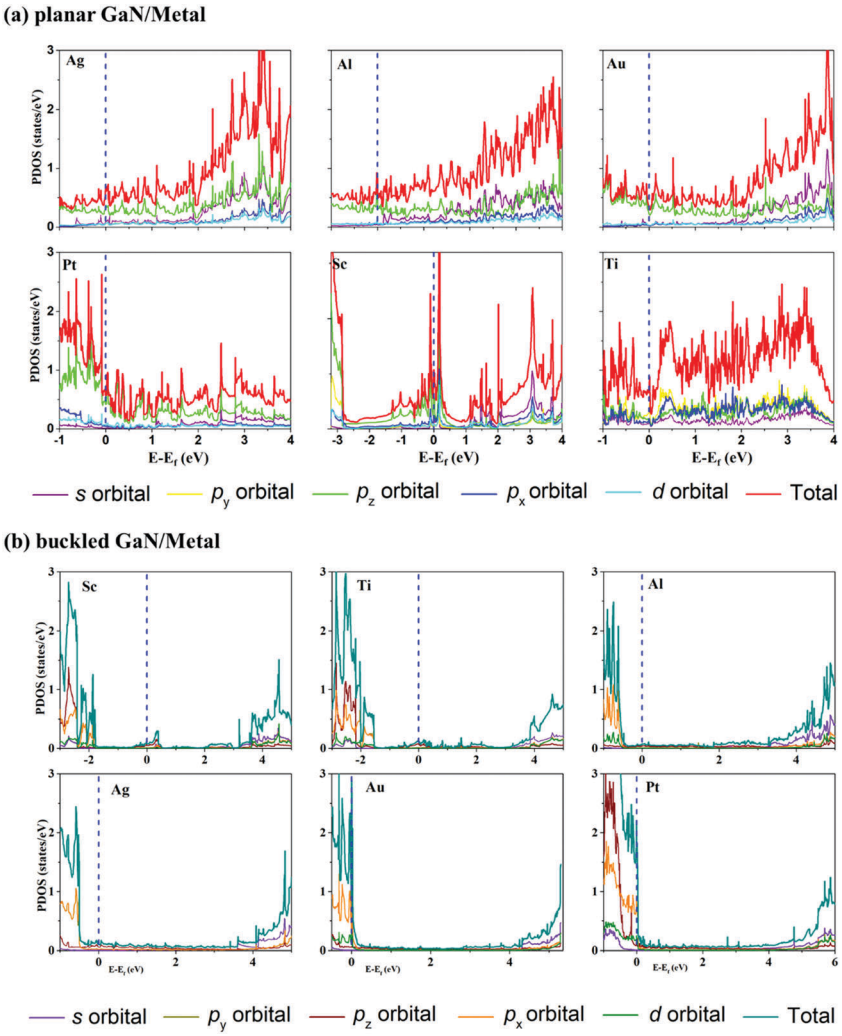

Fig. 6 (a and b) Partial density of states (PDOS) (DOS on ML planar/buckled GaN atom and orbitals) of ML planar/buckled GaN on the Ag, Al, Au, Pt, Sc, and Ti electrodes.

combined systems. Compared with the PDOS of the ML planar GaN/metal combined systems, the band gap of ML buckled GaN is clear (Fig. 6(b)), confirming the semiconductor feature of ML buckled GaN in the combined systems. Hence, a weak van der Waals contact in the vertical direction is formed between ML buckled GaN and the metal electrodes. Near the Fermi level, there is still a small amount of GaN states in the ML buckled GaN/metal combined systems, which is in agreement with the properties of the band structure, as shown in Fig. 5(b) (light purple closed area).

3.2 Quantum transport simulation of the ML GaN FETs

In Fig. 1(e), we present a schematic of an ML GaN FET, and the length of its channel is about 5 nm. In the vertical direction of the ML planar GaN FET, the ML planar GaN is metallized, leading to the absence of a Schottky barrier; however, the Schottky barrier may be in the lateral direction of the ML planar GaN FET. In contrast, the Schottky barrier can appear in both the vertical and lateral directions of the ML buckled GaN FET.

The local density of states (LDOS) in the color coding and transmission spectra of the ML planar GaN FETs with Sc, Ag, Ti, Al, Au, and Pt electrodes are shown in Fig. 7(a). The band bends in the ML planar GaN channel, which reveals that there is an inserted potential, $\Delta\varphi$, induced by the charge transfer in the lateral interface between the channel and source/drain region. The lateral hole (electron) SBH $\Phi_L^{e(h)}$ is the average value between the left and right electron (hole) SBH. As an example, the left and right electron SBH are -0.24 ($\Phi_{L,L}^e$) and 0.24 ($\Phi_{L,R}^e$) eV; thus, the electron SBH is 0 eV for $\Phi_L^e = (\Phi_{L,L}^e + \Phi_{L,R}^e)/2$. The left and right hole SBH are 1.85 ($\Phi_{L,L}^h$) and 1.67 ($\Phi_{L,R}^h$) eV, respectively; thus, the hole SBH is 1.76 eV for $\Phi_L^h = (\Phi_{L,L}^h + \Phi_{L,R}^h)/2$ (Table 2). In terms of the LDOS, the Ag electrode forms an n-type Schottky contact with Φ_L^e = 0.65 eV, and the Ti, Al, and Au electrodes form a p-type Schottky contact with Φ_L^h = 0.40, 0.88, and 1.0 eV, respectively. Remarkably, the Sc/Pt electrodes form an n-type/p-type ohmic contact at the lateral interface.

Because of the band bending in the channel of the ML planar GaN FET, the lateral electron (hole) SBH is not identical with the energy difference between the Fermi level and the

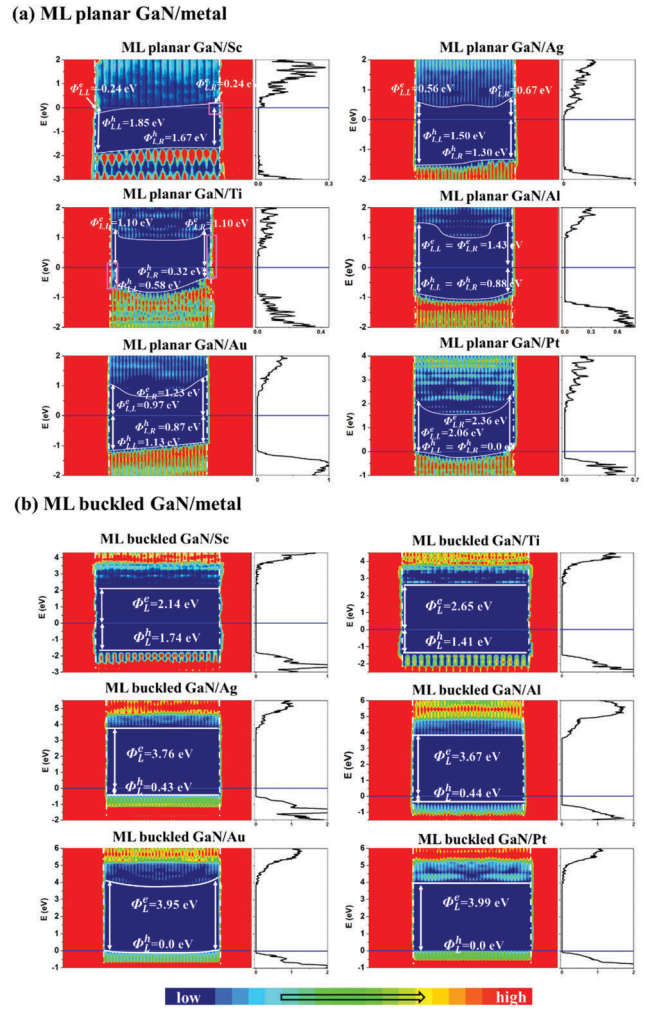

Fig. 7 (a and b) Local density of states (LDOS) in color coding and transmission spectra (TS) of the ML planar/buckled GaN FET with Sc, Ag, Ti, Al, Au, and Pt electrodes under zero-bias and zero-gate voltage, and the channel length is about 5 nm. Light-purple closed area indicates the region with MIGS. The Fermi level is at zero energy. The vertical white dashed lines indicate the boundary of ML GaN/metal and the uncontacted ML GaN channel. The corresponding conduction band and valence band profiles along the channel are given in white lines.

conduction band minimum, CBM, (valence band maximum (VBM)) of the transmission spectra. The semiconducting ML planar GaN is terminated by the metal electrodes and thus, a surface state is probably induced. The observed states appearing in the band gap of planar GaN with Sc and Ti electrodes stem from the MIGS (Fig. 7(a)), and the surface states of the channel planar GaN are responsible for the Fermi level pinning. Moreover, the strong interaction between the metal electrodes alters the band gap of the channel ML planar GaN at the interface and increases the SBH, which is also responsible for the Fermi level pinning. In our model, the channel ML planar GaN is perfect and no defects exist. In actual devices, defects in the channel semiconductor will also lead to Fermi level pinning and reduce the pinning factor.[47]

Fig. 7(b) shows the LDOS in the color coding and transmission spectra of the ML buckled GaN FETs, and there are few

Table 2 Calculated electronic structures of ML GaN–metal contacts. Q is the Mulliken charge per GaN atom transferred from the metal electrodes to ML GaN. Metal work function and W are the work functions for each pure metal electrode and the ML GaN–metal combined systems, respectively. Φ_W^e (Φ_W^h) is the vertical electron (hole) SBH obtained from the work function approximation. $\Phi_{V,B}^e$ ($\Phi_{V,B}^h$) is the vertical electron (hole) SBH obtained from the band calculation. $\Phi_{V,T}^e$ ($\Phi_{V,T}^h$) is the vertical electron (hole) SBH obtained from the transport simulation. Φ_L^e (Φ_L^h) is lateral the electron (hole) SBH obtained from the transport simulation. E_T^L is the transport gap, which is defined as $E_T^L = \Phi_L^e + \Phi_L^h$. The lattice constant and the work function of the free-standing ML planar (buckled) GaN are 3.24 (3.18) Å and 4.74 (5.72) eV, respectively

Metal		Al	Ag	Au	Sc	Ti	Pt
Metal work function (eV)		4.01	4.55	5.28	3.41	3.87	5.66
Planar GaN	Q ($\|e\|$)	−0.047	−0.05	0.017	−0.27	−0.537	−0.02
	W (eV)	4.16	4.20	4.95	3.40	4.26	5.24
	Φ_W^e (eV)	0.51	0.55	1.30	0	0.61	1.59
	Φ_L^e (eV)	1.43	0.65	1.20	0	1.10	2.23
	Φ_W^h (eV)	1.68	1.64	0.89	0	1.58	0.60
	Φ_L^h (eV)	0.88	1.40	1.00	1.76	0.40	0
	E_T^L (eV)	2.31	2.05	2.20	1.76	1.60	2.23
Buckled GaN	Q ($\|e\|$)	0.027	−0.03	0	−0.04	−0.07	−0.02
	W (eV)	5.23	5.77	6.44	4.37	4.74	6.46
	$\Phi_{V,B}^e$ (eV)	3.85	4.01	4.17	3.03	3.03	4.63
	$\Phi_{V,T}^e$ (eV)	3.66	3.62	4.55	3.22	3.15	4.71
	Φ_L^e (eV)	3.67	3.76	3.95	2.14	2.65	3.99
	$\Phi_{V,B}^h$ (eV)	0.44	0.21	0	1.53	1.31	0
	$\Phi_{V,T}^h$ (eV)	0.33	0.48	0	1.41	1.20	−0.33
	Φ_L^h (eV)	0.44	0.43	0	1.74	1.41	0
	E_T^L (eV)	4.11	4.19	3.95	3.88	4.06	3.99

MIGS in terms of the LDOS. Since the conduction and valence bands are flat, the electron/hole SBHs of the ML buckled GaN FETs with Sc, Ti, Ag, Al, and Pt electrodes are the same as that from the transmission spectra. In the lateral direction, the Al, Ag, Ti, and Sc electrodes form a p-type Schottky contact with a hole SBH of 0.43, 0.44, 1.41, and 1.74 eV, respectively. Remarkably, the Au and Pt electrodes form a desirable p-type ohmic contact.

In the lateral direction, the work function approximation (WFA) is used to estimate the SBH of an FET. In the WFA, the energy difference between the E_f of the ML planar GaN/metal combined systems and the CBM/VBM of the channel ML planar GaN determines the lateral electron/hole SBHs, Φ_w^e/Φ_w^h (listed in Table 2). Fig. 8(a) shows the lateral electron/hole SBHs of the ML planar GaN FET produced by the WFA and quantum transport simulations. The contact polarity of the ML planar GaN FET with Ti and Al electrodes is totally opposite in the two ways. The contact type of the ML planar GaN FET with a Pt electrode changes from p-type Schottky contact in the WFA to p-type ohmic contact in the transport simulation. This difference between the WFA and quantum transport simulations is ascribed to the fact that the coupling of ML planar GaN between the electrode and channel regions is completely ignored in the WFA. Consequently, the SBH value in the lateral direction obtained by the WFA is less accurate.[11–13,48–51]

We defined the transport gap to be the total of the electron and hole SBH: $E_T^L = \Phi_L^e + \Phi_L^h$, and the values are 3.88 (Sc),

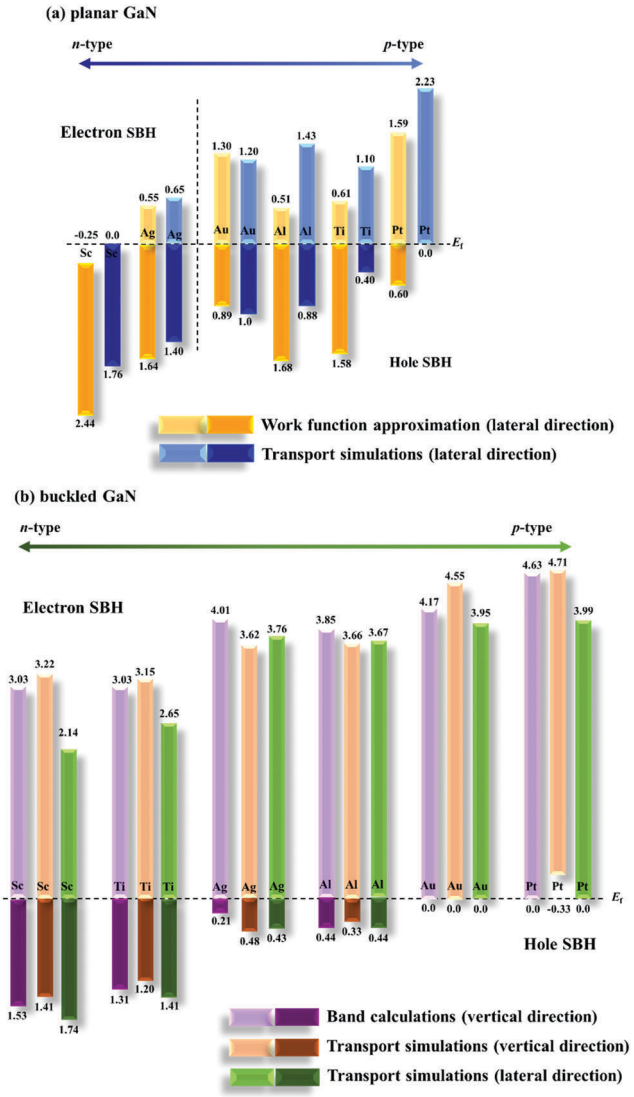

Fig. 8 (a and b) Electron and hole SBHs of the ML GaN on Sc, Ag, Ti, Al, Au, and Pt. The light (deep) blue and yellow rectangle represent the lateral electron and hole SBH obtained from the work function approximation and quantum transport simulations for ML planar GaN, respectively. The light (deep) purple, orange, and green rectangle represent the electron and hole SBH obtained from the band calculations in the vertical direction, quantum transport simulations in the vertical and lateral direction for ML buckled GaN, respectively.

3.95 (Au), 3.99 (Pt), 4.06 (Ti), 4.11 (Al), and 4.19 (Ag) eV. The transport gap is slightly larger than the gap (3.26 eV) from the energy band simulation using the GGA level based on a different plane-wave basis set (VASP). The simulated transport gap should include the many-body effect at the single-electron-approximation-based GGA level, which enlarges the transport gap. Due to charge doping of the metal electrode, the many-electron effect of the channel ML buckled GaN is strongly suppressed and thus, the increase in the transport gap is not significant. Therefore, the actual transport gap is found to be slightly greater than the transport gap simulated at the GGA level. Taking the ML black phosphorene FET as an example, the measured transport gap is 0.99 eV, which is 10% larger than the calculated transport gap (0.91 eV) at the GGA level.[11] The present quantum transport simulation is expected to slightly underestimate the transport gap.

The LDOS projected on ML buckled GaN for the simulated ML buckled GaN transistor with metal electrodes are shown in Fig. S3 (ESI†), and the band gap of ML buckled GaN is identifiable in the electrode region of LDOS. In addition, we could obtain the vertical SBH from the LDOS. The vertical electron/hole SBH is defined as the discrepancy between the Fermi level and the CBM/VBM of ML buckled GaN in the deep electrode region (away from the channel). From the LDOS, p-type Schottky and ohmic contacts remain in both the vertical and lateral directions, and the hole SBH is 0.48/0.43 (Ag), 0.33/0.44 (Al), 1.20/1.41 (Ti), 1.41/1.73 (Sc), 0/0 (Au), and 0/0 eV (Pt). In the electrode region, MIGS are observed in the band gap with the Sc, Ti, Al, Ag, and Pt electrodes. These MIGS adopt electrons from the channel ML buckled GaN near the lateral interface, causing a built-in potential, $\Delta\varphi$; thus, the band of ML buckled GaN in the electrode region bends. As a result, the SBHs defined by the LDOS are somewhat different in the vertical and lateral directions. Fig. 8(b) shows the contrast of the vertical and lateral electron/hole SBHs of the ML buckled GaN FET calculated by the band calculations and quantum transport simulations. The band gaps in the vertical direction are 4.63/4.56 (Sc), 4.35/4.34 (Ti), 4.10/4.22 (Ag), 3.99/4.29 (Al), 4.55/4.17 (Au), and 4.71/4.63 (Pt) eV, which were calculated by the band calculations and quantum transport simulations, respectively. The differences in the SBHs from the three schemes are relatively small.

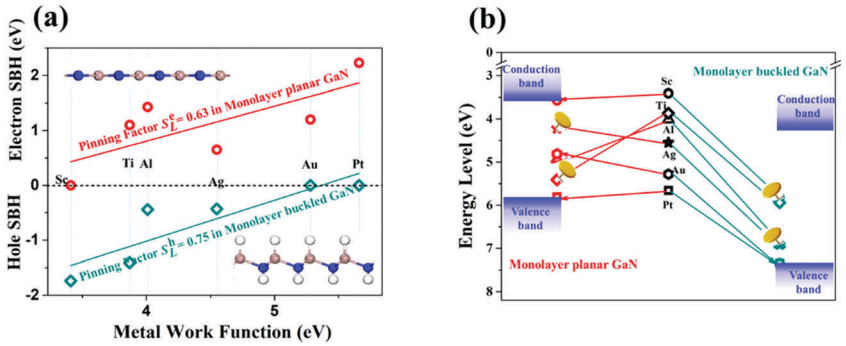

Fig. 9 (a) Lateral electron SBHs for ML planar GaN and hole SBHs for ML buckled GaN using different metal contacts. From the Schottky–Mott rule, S_L^e and S_L^h are the electron and hole pinning factor in the lateral interface between the contacted and uncontacted ML GaN, respectively. Inset: The structure of ML planar and buckled GaN. (b) Illustration of the Fermi level pinning in the ML planar and buckled GaN FETs.

Fig. 9(a) shows the electron SBHs of ML planar GaN and hole SBHs of ML buckled GaN against the metal work function. The slopes of the linear fit to the data are called the electron and hole pinning factors S_L^e and S_L^h, respectively. A complete Fermi-level pinning corresponds to $S = 0$, and no Fermi-level pinning corresponds to $S = 1$.[47] The ML GaN FET has a moderate Fermi-level pinning effect because the calculated pinning of the planar and ML buckled GaN/metal contacts is $S_L^e = 0.63$ and $S_L^h = 0.75$, respectively. These pinning factors are higher than those of ML arsenene ($S_L^e = 0.33$),[48] ML blue phosphorene ($S_L^e = 0.42$),[51] ML BP($S_L^e = 0.28$)[11] and ML bismuthene ($S_L^e = 0.12$)[12] contacted with metals. The weaker Fermi-level pinning effect in ML GaN is ascribed to the small amount of MIGS, as shown in Fig. 7. Fig. 9(b) clearly shows the Fermi-level pinning effect in GaN/metals, and there is an apparent overall downshift in the Fermi level of the metal (about 2 eV) after contact with ML buckled GaN due to the coupling at the interface.[52]

4. Conclusion

In this paper, we report the first comprehensive study on the interfacial properties of ML GaN FET using *ab initio* energy band and quantum transport simulations. In the vertical direction, ML planar GaN undergoes metallization, forming an ohmic contact with metal electrodes. In the lateral direction, because of moderate Fermi level pinning (pinning factor $S_L^e = 0.63$ for electrons), ML planar GaN and the Ag electrode form an n-type Schottky contact with an electron SBH of 0.65 eV, while the Ti, Al, and Au electrodes form a p-type Schottky contact with a hole SBH of 0.40, 0.88 and 1.0 eV, respectively. Remarkably, the Sc/Pt electrodes form a highly desirable n-type/p-type lateral ohmic contact. In the case of the buckled GaN contact to metal electrodes, the energy band structure of ML buckled GaN in the electrode regions is well-maintained due to a vdW interaction. In the vertical/lateral direction, both p-type vertical and lateral Schottky contacts are formed with the Ag, Al, Ti, and Sc electrodes, with a hole SBH of 0.48/0.43, 0.33/0.44, 1.20/1.41, and 1.41/1.73 eV, respectively. There is a moderate pinning factor of $S_L^h = 0.75$ for holes in the lateral direction. Remarkably, the Au and Pt electrodes form a highly desirable p-type ohmic contact in both the vertical and lateral directions. Therefore, a low resistance contact can be realized in ML planar and buckled GaN devices.

Conflicts of interest

There are no conflicts to declare.

Acknowledgements

This study was supported by the National Natural Science Foundation of China (no. 11674005), the National Basic Research Program of China (no. 2016YFB0700600), and the Special Fund of Education Department of Shaanxi Province, China (No. 17JK0138).

References

1 A. K. Singh, H. L. Zhuang and R. G. Hennig, Ab initiosynthesis of single-layer III–V materials, *Phys. Rev. B: Condens. Matter Mater. Phys.*, 2014, **89**(24), 245431.
2 H. L. Zhuang, A. K. Singh and R. G. Hennig, Computational Discovery of Single-layer III-V Materials, *Phys. Rev. B: Condens. Matter Mater. Phys.*, 2013, **87**(16), 165415.
3 R. Dingle, D. D. Sell, S. E. Stokowski and M. Ilegems, Absorption, Reflectance, and Luminescence of GaN Epitaxial Layers, *Phys. Rev. B: Condens. Matter Mater. Phys.*, 1971, **4**(4), 1211–1218.
4 S. Kim, T. H. Seo, M. J. Kim, K. M. Song, E.-K. Suh and H. Kim, Graphene-GaN Schottky diodes, *Nano Res.*, 2014, **8**(4), 1327–1338.
5 Z. Lin, A. McCreary, N. Briggs, S. Subramanian, K. Zhang, Y. Sun, X. Li, N. J. Borys, H. Yuan, S. K. Fullerton-Shirey, A. Chernikov, H. Zhao, S. McDonnell, A. M. Lindenberg, K. Xiao, B. J. LeRoy, M. Drndić, J. C. M. Hwang, J. Park, M. Chhowalla, R. Schaak, A. Javey, M. C. Hersam, J. Robinson and M. Terrones, 2D Materials Advances from Large Scale Synthesis and Controlled Heterostructures to Improved Characterization Techniques, Defects and Applications, *2D Mater.*, 2016, **3**, 042001.
6 M. Tangi, P. Mishra, C. C. Tseng, T. K. Ng, M. N. Hedhili, D. H. Anjum, M. S. Alias, N. Wei, L. J. Li and B. S. Ooi, Band Alignment at GaN/Single-Layer WSe_2 Interface, *ACS Appl. Mater. Interfaces*, 2017, **9**(10), 9110–9117.
7 G. Jo, M. Choe, C. Y. Cho, J. H. Kim, W. Park, S. Lee, W. K. Hong, T. W. Kim, S. J. Park, B. H. Hong, Y. H. Kahng and T. Lee, Large-scale Patterned Multi-layer Graphene Films as Transparent Conducting Electrodes for GaN Light-emitting Diodes, *Nanotechnology*, 2010, **21**(17), 175201.
8 S. Chandramohan, J. H. Kang, B. D. Ryu, J. H. Yang, S. Kim, H. Kim, J. B. Park, T. Y. Kim, B. J. Cho, E. K. Suh and C. H. Hong, Impact of Interlayer Processing Conditions on the Performance of GaN Light-emitting Diode with Specific NiOx/graphene Electrode, *ACS Appl. Mater. Interfaces*, 2013, **5**(3), 958–964.
9 T. H. Seo, K. J. Lee, T. S. Oh, Y. S. Lee, H. Jeong, A. H. Park, H. Kim, Y. R. Choi, E.-K. Suh, T. V. Cuong, V. H. Pham, J. S. Chung and E. J. Kim, Graphene Network on Indium tin Oxide Nanodot Nodes for Transparent and Current Spreading Electrode in InGaN/GaN Light Emitting Diode, *Appl. Phys. Lett.*, 2011, **98**(25), 251114.
10 A. Avramescu, T. Lermer, J. Müller, S. Tautz, D. Queren, S. Lutgen and U. Strauß, InGaN Laser Diodes with 50 mW Output Power Emitting at 515 nm, *Appl. Phys. Lett.*, 2009, **95**(7), 071103.
11 Y. Pan, Y. Wang, M. Ye, R. Quhe, H. Zhong, Z. Song, X. Peng, D. Yu, J. Yang, J. Shi and J. Lu, Monolayer Phosphorene–Metal Contacts, *Chem. Mater.*, 2016, **28**(7), 2100–2109.
12 Y. Guo, F. Pan, M. Ye, X. Sun, Y. Wang, J. Li, X. Zhang, H. Zhang, Y. Pan, Z. Song, J. Yang and J. Lu, Monolayer Bismuthene-Metal Contacts: A Theoretical Study, *ACS Appl. Mater. Interfaces*, 2017, **9**(27), 23128–23140.

13 X. Zhang, Y. Pan, M. Ye, R. Quhe, Y. Wang, Y. Guo, H. Zhang, Y. Dan, Z. Song, J. Li, J. Yang, W. Guo and J. Lu, Three-layer Phosphorene-metal Interfaces, *Nano Res.*, 2018, **11**(2), 707–721.

14 S. B. Desai, S. R. Madhvapathy, A. B. Sachid, J. P. Llinas, Q. Wang, G. H. Ahn, G. Pitner, M. J. Kim, J. Bokor, C. Hu, H.-S. P. Wong and A. Javey, MoS_2 transistors with 1-nanometer gate lengths, *Science*, 2016, **354**(6308), 99–102.

15 Y. Wang, R. X. Yang, R. Quhe, H. Zhong, L. Cong, M. Ye, Z. Ni, Z. Song, J. Yang, J. Shi, J. Li and J. Lu, Does p-type ohmic contact exist in WSe_2-metal interfaces?, *Nanoscale*, 2015, **8**(2), 1179–1191.

16 Y. Wang, P. Huang, M. Ye, R. Quhe, Y. Pan, H. Zhang, H. Zhong, J. Shi and J. Lu, Many-body Effect, Carrier Mobility, and Device Performance of Hexagonal Arsenene and Antimonene, *Chem. Mater.*, 2017, **29**(5), 2191–2201.

17 P. Chen, N. Li, X. Chen, W.-J. Ong and X. Zhao, The rising star of 2D black phosphorus beyond graphene: synthesis, properties and electronic applications, *2D Mater.*, 2017, **5**(1), 014002.

18 Z. Ni, M. Ye, J. Ma, Y. Wang, R. Quhe, J. Zheng, L. Dai, D. Yu, J. Shi, J. Yang, S. Watanabe and J. Lu, Performance Upper Limit of sub-10 nm Monolayer MoS_2 Transistors, *Adv. Electron. Mater.*, 2016, **2**(9), 1600191.

19 J. Kang, W. Liu, D. Sarkar, D. Jena and K. Banerjee, Computational Study of Metal Contacts to Monolayer Transition-Metal Dichalcogenide Semiconductors, *Phys. Rev. X*, 2014, **4**(3), 031005.

20 S. B. Desai, S. R. Madhvapathy, A. B. Sachid, J. P. Llinas, Q. Wang, G. H. Ahn, G. Pitner, M. J. Kim, J. Bokor, C. Hu, H.-S. Philip Wong and A. Javey, MoS_2 transistors with 1-nanometer gate lengths, *Science*, 2016, **354**(6308), 99–102.

21 B. Radisavljevic, A. Radenovic, J. Brivio, V. Giacometti and A. Kis, Single-layer MoS_2 Transistors, *Nat. Nanotechnol.*, 2011, **6**(3), 147–150.

22 A. Nourbakhsh, A. Zubair, R. N. Sajjad, K. G. Amir Tavakkoli, W. Chen, S. Fang, X. Ling, J. Kong, M. S. Dresselhaus, E. Kaxiras, K. K. Berggren, D. Antoniadis and T. Palacios, MoS_2 Field-Effect Transistor with Sub-10 nm Channel Length, *Nano Lett.*, 2016, **16**(12), 7798–7806.

23 K. Xu, D. Chen, F. Yang, Z. Wang, L. Yin, F. Wang, R. Cheng, K. Liu, J. Xiong, Q. Liu and J. He, Sub-10 nm Nanopattern Architecture for 2D Material Field-Effect Transistors, *Nano Lett.*, 2017, **17**(2), 1065–1070.

24 L. Xie, M. Liao, S. Wang, H. Yu, L. Du, J. Tang, J. Zhao, J. Zhang, P. Chen, X. Lu, G. Wang, G. Xie, R. Yang, D. Shi and G. Zhang, Graphene-Contacted Ultrashort Channel Monolayer MoS_2 Transistors, *Adv. Mater.*, 2017, **29**(37), 1702522.

25 Z. Y. Al Balushi, K. Wang, R. K. Ghosh, R. A. Vila, S. M. Eichfeld, J. D. Caldwell, X. Qin, Y. C. Lin, P. A. DeSario, G. Stone, S. Subramanian, D. F. Paul, R. M. Wallace, S. Datta, J. M. Redwing and J. A. Robinson, Two-dimensional Gallium Nitride Realized Via Graphene Encapsulation, *Nat. Mater.*, 2016, **15**(11), 1166–1171.

26 Q. Zhao, Z. Xiong, L. Luo, Z. Sun, Z. Qin, L. Chen and N. Wu, Design of a new two-dimensional diluted magnetic semiconductor: Mn-doped GaN monolayer, *Appl. Surf. Sci.*, 2017, **396**, 480–483.

27 A. K. Singh and R. G. Hennig, Computational Synthesis of Single-layer GaN on Refractory Materials, *Appl. Phys. Lett.*, 2014, **105**, 051604.

28 Z. Qin, G. Qin, X. Zuo, Z. Xiong and M. Hu, Orbitally Driven Low Thermal Conductivity of Monolayer Gallium Nitride (GaN) with Planar Honeycomb Structure: A Comparative Study, *Nanoscale*, 2017, **9**(12), 4295–4309.

29 G. Kresse and D. Joubert, From Ultrasoft Pseudopotentials to the Projector Augmented-wave Method, *Phys. Rev. B: Condens. Matter Mater. Phys.*, 1999, **59**, 1758–1775.

30 G. Kresse and J. Furthmüller, Efficient Iterative Schemes for Ab initio Total-energy Calculations using a Plane-wave Basis Set, *Phys. Rev. B: Condens. Matter Mater. Phys.*, 1996, **54**, 11169–11186.

31 S. Grimme, J. Antony, S. Ehrlich and H. Krieg, A Consistent and Accurate ab initio Parametrization of Density Functional Dispersion Correction (DFT-D) for the 94 Elements H-Pu, *J. Chem. Phys.*, 2010, **132**(15), 154104.

32 S. Grimme, S. Ehrlich and L. Goerigk, Effect of the Damping Function in Dispersion Corrected Density Functional Theory, *J. Comput. Chem.*, 2011, **32**(7), 1456–1465.

33 J. Neugebauer and M. Scheffler, Adsorbate-substrate and Adsorbate-adsorbate Interactions of Na and K Adlayers on Al(111), *Phys. Rev. B: Condens. Matter Mater. Phys.*, 1992, **46**(24), 16067–16080.

34 S. J. Clark, M. D. Segall, C. J. Pickard, P. J. Hasnip, M. I. J. Probert, K. Refson and M. C. Payne, First Principles Methods Using CASTEP, *Z. Kristallogr.*, 2005, **220**, 567–570.

35 M. Segall, P. J. D. Lindan, M. J. Probert, C. J. Pickard, P. J. Hasnip, S. J. Clark and M. C. Payne, First-principles Simulation Ideas, Illustrations and the CASTEP Code, *J. Phys.: Condens. Matter*, 2002, **14**, 2717–2744.

36 R. S. Mulliken, Electronic Population Analysis on LCAOMO Molecular Wave Functions. I, *J. Chem. Phys.*, 1955, **23**(10), 1833–1839.

37 H. Zhong, R. Quhe, Y. Wang, Z. Ni, M. Ye, Z. Song, Y. Pan, J. Yang, L. Yang, M. Lei, J. Shi and J. Lu, Interfacial Properties of Monolayer and Bilayer MoS_2 Contacts with Metals: Beyond the Energy Band Calculations, *Sci. Rep.*, 2016, **6**, 21786.

38 Y. Y. Pan, Y. Y. Wang, L. Wang, H. Zhong, R. Quhe, Z. Ni, M. Ye, W. N. Mei, J. Shi, W. Guo, J. Yang and J. Lu, Graphdiyne-metal Contacts and Graphdiyne Transistors, *Nanoscale*, 2015, **7**(5), 2116–2127.

39 H. Zhong, Z. Ni, Y. Wang, M. Ye, Z. Song, Y. Pan, R. Quhe, J. Yang, L. Yang, J. Shi and J. Lu, Interfacial Properties of Monolayer and Bilayer MoS_2 Contacts with Metals: Depressed Many-electron Effects, *Sci. Rep.*, 2015, **6**, 21786.

40 Y. Wang, R. X. Yang, R. Quhe, H. Zhong, L. Cong, M. Ye, Z. Ni, Z. Song, J. Yang, J. Shi, J. Li and J. Lu, Does p-type Ohmic Contact Exist in WSe_2-metal Interfaces?, *Nanoscale*, 2016, **8**(2), 1179–1191.

41 Q. Li, J. Yang, R. Quhe, Q. Zhang, L. Xu, Y. Pan, M. Lei and J. Lu, Ohmic contacts between monolayer WSe 2 and two-dimensional titanium carbides, *Carbon*, 2018, **135**, 125–133.

42 S. Das, W. Zhang, M. Demarteau, A. Hoffmann, M. Dubey and A. Roelofs, Tunable transport gap in phosphorene, *Nano Lett.*, 2014, **14**(10), 5733–5739.
43 Y. Pan, Y. Wang, M. Ye, R. Quhe, H. Zhong, Z. Song, X. Peng, J. Li, J. Yang, J. Shi and J. Lu, Monolayer Phosphorene-Metal Interfaces, *Chem. Mater.*, 2016, **28**(7), 2100–2109.
44 J. Qiao, X. Kong, Z.-X. Hu, F. Yang and W. Ji, High-mobility Transport Anisotropy and Linear Dichroism in Few-layer Black Phosphorus, *Nat. Commun.*, 2014, **5**, 4475.
45 Y. Cai, G. Zhang and Y.-W. Zhang, Layer-dependent Band Alignment and Work Function of Few-layer Phosphorene, *Sci. Rep.*, 2014, **4**, 6677.
46 S. Das, W. Zhang, M. Demarteau, A. Hoffmann, M. Dubey and A. Roelofs, Tunable Transport Gap in Phosphorene, *Nano Lett.*, 2014, **14**(10), 5733–5739.
47 Y. Liu, J. Guo, E. Zhu, L. Liao, S. J. Lee, M. Ding, I. Shakir, V. Gambin, Y. Huang and X. Duan, Approaching the Schottky-Mott limit in van der Waals metal-semiconductor junctions, *Nature*, 2018, **557**(7707), 696–700.
48 Y. Wang, M. Ye, M. Weng, J. Li, X. Zhang, H. Zhang, Y. Guo, Y. Pan, L. Xiao, J. Liu, F. Pan and J. Lu, Electrical Contacts in Monolayer Arsenene Devices, *ACS Appl. Mater. Interfaces*, 2017, **9**(34), 29273–29284.
49 Y. Wang, J. Li, J. Xiong, Y. Pan, M. Ye, Y. Guo, H. Zhang, R. Quhe and J. Lu, Does the Dirac cone of germanene exist on metal substrates?, *Phys. Chem. Chem. Phys.*, 2016, **18**(28), 19451–19456.
50 Y. Guo, F. Pan, M. Ye, Y. Wang, Y. Pan, X. Zhang, J. Li, H. Zhang and J. Lu, Interfacial properties of stanene–metal contacts, *2D Mater.*, 2016, **3**(3), 035020.
51 J. Li, X. Sun, C. Xu, X. Zhang, Y. Pan, M. Ye, Z. Song, R. Quhe, Y. Wang, H. Zhang, Y. Guo, J. Yang, F. Pan and J. Lu, Electrical contacts in monolayer blue phosphorene devices, *Nano Res.*, 2018, **11**(4), 1834–1849.
52 J. Zheng, Y. Wang, L. Wang, R. Quhe, Z. Ni, W. N. Mei, Z. Gao, D. Yu, J. Shi and J. Lu, Interfacial Properties of Bilayer and Trilayer Graphene on Metal Substrates, *Sci. Rep.*, 2013, **3**, 02081.